International Journal of Nanomedicine

Dovepress
Taylor & Francis Group

Open Access Full Text Article

ORIGINAL RESEARCH

Integrated Colorisensing Platform with Microneedles and Metal-Phenol Nanozymes for Point-of-Care Testings of Acetylcholinesterase Activity and Its Drug Inhibitor

Erlin Chen[1], Peng Chang[2], Haibin Xu[2], Hongxing Xu[2], Zhiqiang Zhu[3], Danfeng Shen[2]

[1]Department of General Surgery, Affiliated Hospital of Nantong University, Medical College of Nantong University, Nantong, 226000, People's Republic of China; [2]Department of General Surgery, Taicang Affiliated Hospital of Soochow University, Suzhou, 215400, People's Republic of China; [3]School of Biomedical Sciences, Suzhou Chien-Shiung Institute of Technology, Suzhou, 215411, People's Republic of China

Correspondence: Danfeng Shen; Hongxing Xu, Department of General Surgery, Taicang Affiliated Hospital of Soochow University, Suzhou, 215400, People's Republic of China, Email danfengsh@hotmail.com; hongxingxu0601@hotmail.com

Introduction: The detection of acetylcholinesterase (AChE) activity and the screening of its inhibitors are of significant importance for the diagnosis and drug therapy of nervous system diseases, particularly neurodegenerative disorders. This study aimed to develop a novel, integrated point-of-care testing (POCT) platform to address this need.

Methods: We designed and integrated a colorimetric biosensor (Colorisensor) that combines a microneedle array with a metal-phenol nanozyme. The core sensing element is Iron (III)-polydopamine (Fe-PD) nanorods, which exhibit high peroxidase-like activity. The detection mechanism is based on the AChE-catalyzed hydrolysis of acetylthiocholine (ATCh) to produce thiocholine (TCh), which inhibits the nanozyme's activity. This inhibition prevents the catalytic oxidation of the chromogenic substrate TMB, leading to a measurable color change. A smartphone was utilized to quantify this change via red, green, and blue (RGB) values, creating a rapid and user-friendly platform for detections of AChE activity and its drug inhibitor. The nanorods and microneedle arrays were characterized using scanning electron microscopy, high-resolution transmission electron microscopy, energy-dispersive X-ray spectroscopy, ultraviolet-visible spectrophotometer, water absorption expansion rate, as well as mechanical property tests.

Results and Discussion: The proposed Colorisensor demonstrated excellent analytical performance, including high selectivity and sensitivity with a low detection limit (LOD) of 0.007 mU/mL and a broad linear range from 0.01 to 1000 mU/mL. It was successfully applied to screen berberine hydrochloride as an AChE inhibitor. Crucially, the Colorisensor showed comparable accuracy to the standard Ellman's method and outperformed both traditional assays and emerging nanomaterial-based colorimetric methods by offering a wider detection range and a lower LOD.

Conclusion: This study presents a successful proof-of-concept for an integrated microneedle and nanozyme-based Colorisensor. The platform provides a viable and promising alternative pathway for the early diagnosis of neurodegenerative diseases and the screening of therapeutic drugs, highlighting its significant potential for point-of-care applications.

Plain Language Summary:

- Facile Fe-PD nanorods hold high POD-like catalyticity for AChE colorimetric analysis.
- High sensitivity and accuracy could be achieved by nanozyme-based Colorisensors.
- Microneedle array integration enables point-of-care testings of AChE and berberine.

Keywords: microneedle, metal-phenol nanozyme, point-of-care testings, acetylcholinesterase, drug inhibitor, colorimetric sensor

Received: 25 September 2025
Accepted: 1 December 2025
Published: 7 December 2025

Introduction

Acetylcholinesterase (AChE), an essential enzyme in the cholinergic nervous system, is responsible for breaking down the neurotransmitter acetylcholine (ACh) into choline and acetate, thereby modulating the levels of ACh at synapses in a dynamic manner.[1,2] Dysregulation of AChE activity—whether excessive or deficient—is closely associated with severe neurological disorders. Notably, enhanced AChE activity leads to the depletion of ACh, a hallmark of neurodegenerative diseases such as Alzheimer's disease (AD), Parkinson's disease, and Huntington's disease.[3] Conversely, elevated ACh accumulation due to suppressed AChE activity can disrupt neurotransmission, potentially resulting in fatal outcomes.[4] Given its central role in neuroregulation, AChE has emerged as a key biomarker for neurodegenerative conditions,[5] particularly AD, where its activity is significantly elevated in patients. Consequently, AChE inhibitors have garnered substantial attention as potential therapeutic agents for AD treatment. The development of highly sensitive and efficient biosensors to detect AChE activity and evaluate inhibitor efficacy is thus imperative—not only for early diagnosis of neurodegenerative diseases but also for accelerating drug discovery and personalized therapeutic strategies.

Various sensing strategies have been developed for detecting AChE activity or screening its inhibitors, including colorimetric assays,[6] fluorescent assays,[7] chromatography-mass spectrometry,[8] electrochemical sensors,[8] and others. Among these, colorimetric analysis has gained significant attention in AChE activity assays due to its convenience, low cost, fast readout, ease of visual detection, and strong potential for point-of-care or ready-to-use applications.[9,10] Nowadays, colorimetric detections of acetylcholinesterase and its drug inhibitors have been developed using molecularly imprinted polymers,[11] nanomaterials,[12] antibodies,[13] and natural enzymes[14] as recognition units. Nanoenzymes are a series of biological nanomaterials with enzyme-like catalytic capabilities, which have many advantages such as high catalytic activity, low cost, and ease of large-scale preparation.[15,16] In addition, nanoenzymes also overcome some limitations of natural enzymes, such as low tolerance to pH, temperature, and organic solvents, impaired activity during long-term use, and difficult purification.[17] For example, Lin's research group prepared manganese dioxide (MnO_2) nanosheets as an oxidase-mimicking nanomaterial, which could directly oxidize TMB into oxTMB without the need for horseradish peroxidase (HRP) and H_2O_2,[18] supporting the colorimetric detection of acetylcholinesterase activity and its inhibitor. Other biomimetic enzyme-like nanomaterials, such as 2D Zn-TCPP(Fe) nanosheets,[1] α-FeOOH nanorods,[19] and FeMn DSAs/N-CNTs nanozymes,[20] are also employed to develop colorimetric biosensors for the detection of AChE and its inhibitor. Although great progress in nanozyme-based colorimetric sensors has been made, it is necessary to develop a real-time, on-site, and portable approach for AChE detection and inhibitor screening. Amazingly, the development of microneedle-mediated POCT strategies hinges on the synergistic integration of biosensing and biofluid sampling. On one hand, the emergence of highly sensitive microneedle-mediated biosensors allows for the direct transduction of biochemical signals in the dermal layers, paving the way for novel closed-loop diagnostic systems.[21] For instance, Ruan et al constructed a dual-continuous microneedle patch integrating transdermal delivery of pH-sensitive licorzinc MOFs and Zn^{2+} hydrogel sensors for managing alopecia areata.[22] Meanwhile, these microneedle-based biosensors are powerfully complemented by substantial progress in using microneedles to efficiently extract interstitial fluid,[23–25] which establishes a reliable, minimally invasive method to obtain a rich source of biomarkers, making subsequent laboratory-grade analysis possible at the point-of-care. Therefore, the integration of microneedle-mediated POCT strategies into nanozyme-based colorimetric sensors probably offer a potential approach for on-site monitoring of AChE in interstitial fluid, heralding a new era in point-of-care diagnostics of neurodegenerative diseases. A key advantage of this POCT platform is its ability to provide rapid, real-time feedback on AChE levels through minimally invasive sample analysis, enabling immediate clinical or therapeutic decision-making at the point of sampling.[26] This capability empowers healthcare providers to optimize treatment protocols and monitor disease progression dynamically. Moreover, the developing smartphone-assisted POCT colorimetric system streamlines traditional AChE detection workflows, effectively shifting the diagnostic paradigm from centralized laboratories to decentralized settings such as clinics or even home care conditions. Importantly, this microneedle-based user-friendly smart POCT colorimetric sensor not only enhances patient engagement in biomarker monitoring but also supports data-driven choices for personalized healthcare interventions.[27,28]

To achieve this aim, we ingeniously designed and constructed a portable Colorisensor coupling with microneedle and metal-phenol nanozyme for smartphone-assisted point-of-care testings of acetylcholinesterase activity and its drug inhibitor (Scheme 1). When pressing the microneedle array for contacting with the skin layer, the analytes in ISF could respond to Fe-PD nanozymes. In the presence of AChE, it catalytically hydrolyzes ATCh into TCh. With its high reducing ability, TCh induces the decomposition of Fe-PD nanozymes, causing the inhibition of their POD-like activity. Hence, with the increasing concentration of AChE, there is an apparently fading change in the color of the oxTMB solution oxidized by H_2O_2 under the catalysis of Fe-PD nanozymes. Furthermore, to make the detection more smart, convenient, and minimally invasive, we have combined colorimetric methods with microneedle technology and an RGB identification strategy to create a colorimetric microneedle-mediated biosensing array for intelligent detection of AChE activity and its inhibitors. The developed Colorisensor exhibits outstanding sensitivity, selectivity, repeatability, and long-term stability, which hold promising prospects in the early diagnosis and screening of therapeutic drugs for neurodegenerative diseases.

Materials and Methods

Reagents and Materials

Dopamine hydrochloride (DA·HCl), iron(III) chloride hexahydrate ($FeCl_3 \cdot 6H_2O$), hydrogen peroxide (H_2O_2), 3,3′,5,5′-tetramethylbenzidine (TMB), acetylcholinesterase (AChE), acetylthiocholine iodide (ATCh), berberine hydrochloride, potassium chloride (KCl), glucose (Glu), L-cysteine (L-Cys), glutathione (GSH), glucoseoxidase (GOx), lysozyme (Lyz), tyrosinase (Tyr), N-vinylpyrrolidone (NVP), ethoxylated trimethylolpropane triacrylate (ETPTA), 2-hydroxy-2-methyl-propiophenone (HMPP), ethylene glycol dimethacrylate (EGDMA), 1×PBS buffer (pH=7.4), acetic acid (HAc), and sodium acetate (NaAc) were purchased from NanJing WanQing Chemical Glassware Instrument Co., Ltd. All chemicals were of analytical grade and used without further purification. All porcine ear skin samples were collected from healthy male domestic pigs, aged 8 months and weighing ~100 kg, obtained from a local market. The sacrifice of the pigs were not involved in this study. These specific sources and application basis of porcine skins were stated in Source Declaration of Porcine Ear Skin.

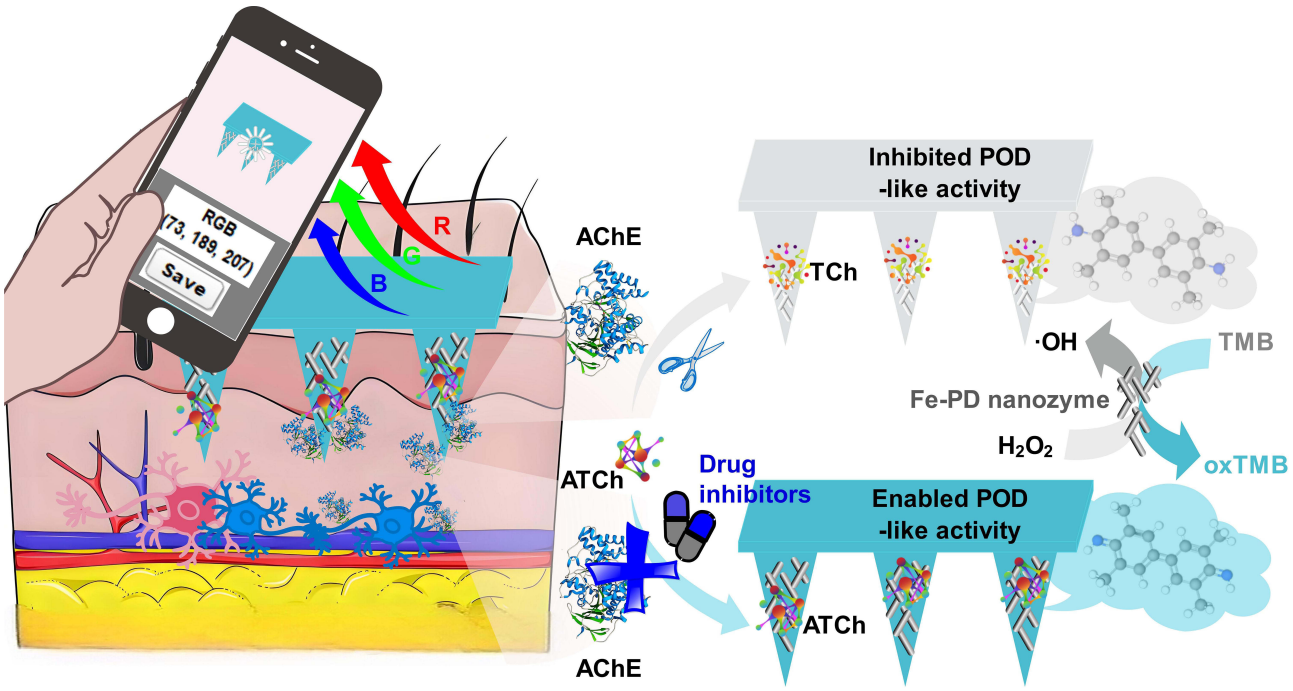

Scheme 1 Schematic illustration of point-of-care testings of acetylcholinesterase activity and its drug inhibitor by the integrated smart color-sensing platform with microneedle arrays and metal-phenol nanozymes.

https://doi.org/10.2147/IJN.S565467

Preparation and Characterization of Fe-PD Nanozymes

To synthesize Fe-PD nanozymes, $NH_3 \cdot H_2O$ was initially added to a conical flask containing a mixture of ethanol and deionized water (2/8, v/v), followed by stirring for 1 hour until the solution became homogeneous at a pH of 10. Subsequently, solutions of DA (15 mL, 50 mg/mL) and $FeCl_3 \cdot 6H_2O$ (5 mL, 50 mg/mL) were sequentially introduced into the aforementioned flask. The reaction solution was maintained at room temperature and stirred for 7 hours. Thereafter, the resulting Fe-PD product was subjected to centrifugation (13500 rpm, 30 min) and washed three times with deionized water and ethanol, respectively. Ultimately, the Fe-PD nanozymes were dried at 45 °C.

The morphology and chemical composition of the synthesized Fe-PD nanozymes were thoroughly characterized using various analytical techniques. Scanning electron microscopy (SEM, Hitachi S4800) was employed to investigate the nanozymes' structural features at an accelerating voltage of 5.0 kV, a beam current of 10 μA, and a working distance of 13.5 mm, with micrographs captured at a magnification of 30.0k. The detailed morphology and elemental composition of the nanozymes were analyzed using high-resolution transmission electron microscopy (HRTEM) and energy-dispersive X-ray spectroscopy (EDX) on an FEI Talos 200x instrument. The analysis was conducted in STEM mode with a high tension of 200 kV. Key parameters for the EDX spectrum imaging included a beam convergence of 10.5 rmad, a camera length of 98 mm, a spot size of 5, and a dwell time of 10.0 μm. The spectrum image was acquired at a magnification of 261kx with an image size of 1024×1024 pixels over 24 frames. The UV-Vis absorption spectrum of the Fe-PD nanozyme-based colorimetric system was recorded using an ultraviolet-visible spectrophotometer (UV-Vis, Shanghai MAPADA). The UV-Vis absorption spectra within the range of 550–750 nm were recorded at 25 °C. Quantitative analysis was performed based on the maximum absorption peak observed at 652 nm. Additionally, the zeta potential was measured with a laser particle size analyzer (Brookhaven, ZetaPALS) to evaluate the surface charge of the nanozymes.

Enzyme-Like Activity and Steady-State Kinetics of Fe-PD Nanozymes

The Enzyme-like activity of Fe-PD nanozymes was evaluated by the system, including Fe-PD (50 μL, 50 μg/mL), TMB (100 μL,2 mM), and H_2O_2 (100 μL, 10 mM) in the NaAC-HAC buffer (0.1 M, pH 4.0). After incubation for 6 minutes at 37 °C, UV-Vis absorption spectra were recorded at 652 nm, and corresponding photographs were taken to visually assess the reaction process. Steady-state kinetic analysis of Fe-PD nanozymes was conducted by varying the substrate concentrations of TMB (0.05 mM to 8.0 mM) and H_2O_2 (0.125 mM to 32.0 mM), while keeping the concentration of Fe-PD nanozymes constant. Absorbance spectra of the solutions were recorded at 652 nm. The Michaelis-Menten constant (K_m) and the maximum reaction velocity (V_{max}) were then calculated using the Michaelis-Menten equation, based on the relationship between substrate concentrations and reaction velocity.[29,30]

Colorimetric Detection of AChE Activity and Its Inhibitor

According to previous studies,[31,32] the enzymatic activity of AChE and its inhibition by berberine hydrochloride were evaluated using a colorimetric assay of an aqueous TMB + H_2O_2 system. The assay was based on the oxidation of TMB catalyzed by Fe-PD nanozymes in the presence of H_2O_2, with the enzymatic hydrolysis product thiocholine (TCh) serving as an inhibitor of the oxidation reaction. Then, Fe-PD suspension (0.05 mg/mL in acetate buffer, pH 4.0), TMB solution (2 mM in ethanol), H_2O_2 solution (10 mM in deionized water), AChE solution (0.1–1000 mU/mL in PBS, pH 7.4), ATCh solution (30 mM in PBS), NaAc-HAc buffer (0.1 M, pH 4.0) were prepared. To validate the sensing mechanism, five control experiments were conducted: Group a (Control): NaAc-HAc buffer only. Group b (Fe-PD + H_2O_2 + TMB): To confirm TMB oxidation by Fe-PD/H_2O_2. Group c (Fe-PD + H_2O_2 + TMB + AChE): To assess AChE's direct effect. Group d (Fe-PD + H_2O_2 + TMB + ATCh): To examine ATCh interference. Group e (Fe-PD + H_2O_2 + TMB + AChE + ATCh): To verify TCh-mediated inhibition of TMB oxidation. Then, different concentrations of AChE (0.01–1000.0 mU/mL) were incubated with ATCh (5 mM, 20 min, 37°C) to generate TCh. The reaction mixture was then added to a solution containing Fe-PD, H_2O_2, and TMB. The absorbance at 652 nm (oxTMB) was recorded using a UV-Vis spectrophotometer. To evaluate inhibitory effects, varying concentrations of berberine hydrochloride (0.1–150 μM) were pre-incubated with AChE (50 mU/mL) for 15 min at 37°C before adding ATCh. The residual AChE activity was determined by measuring the UV-Vis absorbance peak intensity at 652 nm from the suppression of TMB oxidation.

Construction of Microneedle-Based Colorimetric Sensing Array and Characterizations of the Micronnedle Patch

First, 23.75 mg of 3A-PBA, 750 μL of NVP, 100 μL of ETPTA, and 19 μL of EGDMA were added to a centrifuge tube, followed by shaking and ultrasonic treatment until the solution was thoroughly dissolved. Then, 9 μL of HMPP was added as a photoinitiator, and the mixture was shaken to ensure complete blending. The resulting solution was carefully injected into a designed polydimethylsiloxane (PDMS) microneedle mold (depth: 800 μm, base width: 400 μm, center space: 900 μm and placed in a vacuum chamber for 5 minutes. Subsequently, photo-crosslinking was performed under UV light (360 nm, 5 W) to form the microneedle array. The microneedle array was then carefully removed from the PDMS mold and stored in a desiccator for future use. Microneedle arrays were first incubated in Fe-PD nanozyme solution (0.05 mg/mL) for 1 h to allow boronate ester bond formation, then rinsed with PBS to remove unbound nanozymes. For ATCh loading, the above pre-functionalized microneedle arrays were incubated in the 30 mM ATCh solution for 30 min and dried under nitrogen.

For the microneedle characterization, SEM imaging was performed under an accelerating voltage of 5.0 kV and a beam current of 10 μA, with a working distance of 18.5 mm, a stage tilt of 30°, and a magnification of 50. The demolding rate was calculated following the defined equation 1:

$$\text{Demolding rate}(\%) = \frac{\text{No.}_{\text{Demolded microneedles}}}{\text{No.}_{\text{Designed microneedles}}} \times 100\%$$

Where $\text{No.}_{\text{Demolded microneedles}}$ represents the number of needles in the demolded microneedle patch, and $\text{No.}_{\text{Designed microneedles}}$ represents the number of needles in the designed microneedle mold.

For the mechanical hardness of the microneedles, we positioned the microneedle patch on the sample stage of a single-column material testing machine (Instron 5940). Relevant test parameters were configured prior to the experiment, and the compression table was carefully adjusted to achieve proper clamping of the microneedle patch. Subsequently, a compression test was performed at a constant speed of 1.0 mm/min to determine the corresponding compressive mechanical curve.

The microneedle array was immersed in 1× PBS solution (pH 7.4), and its weight was recorded at various soaking time points (0 min, 1 min, 3 min, 5 min, 7 min, 10 min, 20 min, 30 min, 60 min). According to the previous reference,[33] the water absorption expansion rate was calculated following the equation 2:

$$\text{Water absorption expansion rate}(\%) = \frac{W_s - W_0}{W_0} \times 100\%$$

Where Ws is the weight of the microneedle patch after swelling, and W_0 is the initial weight of the microneedle patch.

POCT Analysis of AChE and Its Drug Inhibitor in Simulated Samples

Before detection, fresh porcine ear skin purchased from the local market were used as model samples simulating human skin and processed through the following steps: (1) The pig skin was disinfected with 75% ethanol, followed by cleaning with phosphate-buffered saline (PBS, 10 mM, pH 7.4) to remove surface contaminants; (2) The clean skin was cut into uniform small pieces and incubated overnight at 4°C in an artificial interstitial fluid (AISF) containing different concentrations of AChE (1, 10, 100, 1000 mU/mL) and varying concentrations of berberine (0.1, 10, 20, 40, 80, 120, 160 μM); (3) After incubation, the excess liquid on the surface of the skin sample, containing the AChE or its inhibitor-AISF complex, was gently blotted with a lint-free cloth. This pre-treatment ensured the uniform distribution of AChE or its inhibitor in the dermal matrix, thereby ensuring the accuracy of the subsequent detection results. Next, the engineered nanozyme-based microneedle Colorisensor patches were pressed onto the surface of the pre-treated porcine skin. After 20 minutes of contact, the patches were immersed in TMB (2 mM, 1000 μL) and H_2O_2 (10 mM, 1000 μL) for 3 minutes. The patches were then removed, and the color change of the patches was observed. The RGB values of the patches were measured using a color detection app on a smartphone.

Statistical Analysis

Statistical analysis of the data was performed using GraphPad Prism 10 Software. All data were presented as the mean ± the standard deviation (SD). Specifically, Tukey's multiple comparison test was employed to further elaborate on significant differences among various groups. The data were marked as (*) $P < 0.05$, (**) $P < 0.01$, (***) $P < 0.001$, and (****) $P < 0.0001$. The P-value above 0.05 was considered non-significant (^{ns}).

Results and Discussions

Preparation and Characterization of Fe-PD Nanorods

To our knowledge, dopamine tends to form the 0D sphere or 2D film when metal and ligands undergo cross-linking.[34,35] In this study, we employed a novel approach through Fe (III)-catechol coordination interaction, producing Fe-PD nanorods that served as catalytic components of the POCT colorimetric sensor. Our template-free strategy has overcome key issues in the fabrication process of nanorod-structured synthesized enzymes, including complicated experimental routines, strict conditions, long time-consuming, difficult removal, and residual side effects of the template.[36] To prepare Fe-PD nanorods, dopamine and Fe^{3+} were successively added for chelation in an alkaline ethanol/water reaction system (Figure 1A). During the reaction stage, the catechol groups of dopamine can strongly chelate and cross-link with Fe to form Fe-PD precursor.[37,38] These chemical chelates were further aggregated and polymerized by radical polymerization, resulting in Fe-PD nanorods for the next step of ATCh sensing. The SEM images in Figure 1B and C exhibited the

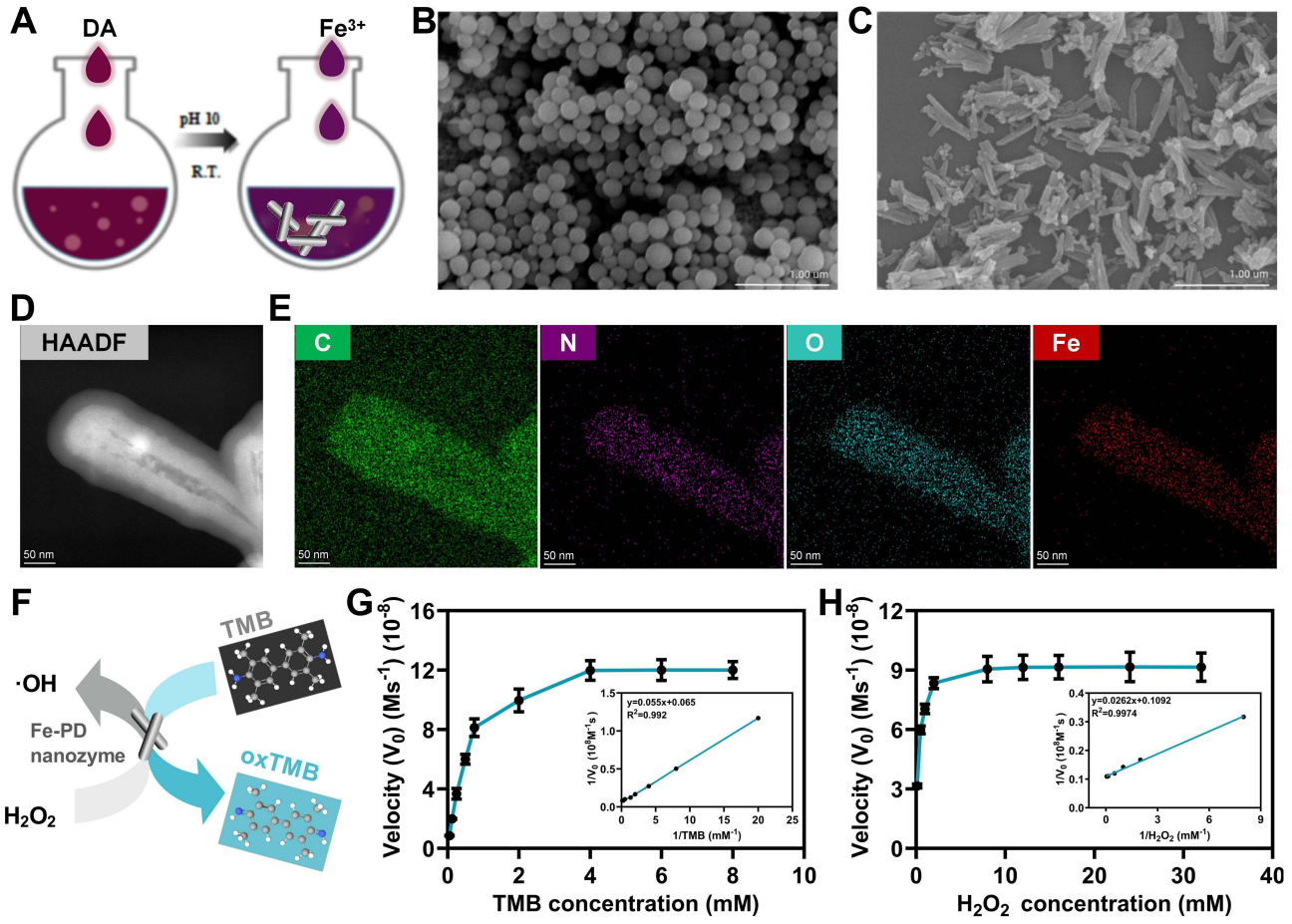

Figure 1 (**A**) The synthesis procedure of Fe-PD nanozymes. (**B**) The SEM image of the initial coordinated Fe-PD nanospheres; (**C**) The SEM image of the finally prepared Fe-PD nanorods. (**D**) HAADF-STEM image of Fe-PD nanorods. (**E**) EDS mapping of the Fe-PD nanorods. (**F**) Schematic illustration of the POD-like catalytic process of Fe-PD nanozymes. (**G**) Kinetics for POD-like activity of Fe-PD nanozymes with different concentrations of TMB (0.05–8 mM). Inset: Corresponding Lineweaver-Burk plot with a resulting linear equation of y = 0.055x + 0.065 (R^2 = 0.9992). (**H**) Kinetics for POD-like activity of Fe-PD nanozymes with different concentrations of H_2O_2 (0.125–32.0 mM). Inset: Corresponding Lineweaver-Burk plot with a resulting linear equation of y = 0.0262x + 0.1092 (R^2 = 0.9974).

change of the resulting DA-Fe chelates from nanospheres to nanorods. The Fe-PD nanorods were synthesized with a length of about 346.0 nm and a diameter of about 88.2 nm in a mold alkaline environment, as shown in the high-angle angular dark field-scanning transmission electron microscope (HAADF-STEM) image of Figure 1D. The EDS spectroscopy characterization (Figure 1E and Table S1 in Supporting Information) indicated that ≈6.0 wt% Fe element is uniformly distributed in the Fe-PD nanorods, which means effective Fe (III) chelate with dopamine molecules. Meanwhile, the zeta potential of the Fe-PD+ nanorods was measured at −17.2 mV, representing a notable positive shift compared to pristine PDA (−38.7 mV) (Figure S1). These findings collectively confirm the successful formation of Fe-PD nanorods.

Afterwards, potential possibilities of Fe-PD nanorods were investigated for the role of nanozymes in POCT colorimetric sensors. Herein, to determine the enzymatic-like activity of Fe-PD nanorods, we further studied their enzymatic catalytic behavior using the TMB-H_2O_2 reaction system. Generally, peroxidase can catalyze colorless TMB to produce blue oxTMB by generating active hydroxyl radicals in the presence of H_2O_2,[39] accompanied by the appearance of a characteristic absorption peak at 652 nm.[40] To systematically evaluate the catalytic efficiency of Fe-PD nanorods as nanoenzymes (Figure 1F), we conducted steady-state kinetic parameter analysis, including the Michaelis constant (K_m) and maximum reaction rate (V_{max}). By adjusting the concentrations of TMB and H_2O_2, the steady-state kinetics were investigated to better understand the enzyme-like activity of the prepared Fe-PD nanorods. In Figure 1G and H, Fe-PD nanorods exhibit typical Michaelis-Menten models at different concentrations of TMB and H_2O_2, respectively. Moreover, when changing the concentration of the other substrate, Lineweaver-Burk curves can be obtained (Insets of Figure 1G and H). The resulting K_m value and V_{max} of Fe-PD nanorods were evaluated by fitting the Lineweaver-Burk equation in the double reciprocal plot. The K_m of Fe-PD nanorods for TMB and H_2O_2 are calculated as 0.85 and 0.24 mM, respectively. Its K_m (TMB) value is lower compared to that of the HRP [K_m (TMB): 0.43 mM]; meanwhile, its K_m (H_2O_2) value is smaller than that of the HRP [K_m (H_2O_2): 3.7 mM].[41] Additionally, when using the TMB as the substrate, Fe-PD nanorods achieved a stronger affinity with higher catalytic efficiency (V_{max} = 15.38×10^{-8} MS^{-1}) compared to that of previously reported other nanozymes using TMB as substrate (Table S2). Further, this nanorod-structured Fe-PD enzyme exhibits outstanding affinity with a higher maximum reaction rate (9.16×10^{-8} MS^{-1}) when using H_2O_2 as the substrate, which exceeds most of the counterpart nanozymes (Table S3). The outstanding POD-like activity of the Fe-PD nanozyme is attributed to its three-dimensional rod-shaped structure (as illustrated in Figure 1C) and numerous catalytic sites, significantly promoting electron transfer.[42] The inclusion of Fe^{3+} serves to reconfigure the electronic distribution,[43] further enhancing its POD-like activity. More importantly, Fe-PD nanorods, as metal-catechol ligand cross-linking nanomaterials, could maintain their enzymatic-like catalytic activity over a long time with a low RSD value of 1.06% and attenuation rate less than 3.0% (until 85 days, Figure S2). These exciting results indicate the stronger affinity and catalytic activity of Fe-PD nanozymes than natural HRP and other reported POD-like nanozymes, with excellent practical stability. This further proves that Fe-PD nanozymes have reliable POD-like behavior, and this preparation approach could be advantageous for practical applications.

Analytical Performance of This Colorisensor for AChE

Taking advantage of excellent POD-like activity, Fe-PD nanozymes could effectively catalyze the oxidation of colorless TMB (Curve a in Figure 2A) to produce the blue oxTMB (Curve b in Figure 2A) in the presence of hydrogen peroxide, resulting in a marked increase in absorbance at 652 nm. Experimental results showed that the only addition of AChE (Curve c in Figure 2A) or ATCh (Curve d in Figure 2A) had no significant impact on the absorbance of the system, indicating that these components did not interfere with the colorimetric assay. As shown in Figure 2A-Curve e and Figure 2B, when both AChE and ATCh were present in the system (with their pre-reaction producing TCh), the absorbance significantly decreased, suggesting that TCh generated by AChE-catalyzed hydrolysis of ATCh could effectively inhibit the catalytic activity of Fe-PD nanozymes and prevent the oxidation of TMB. These findings demonstrate that the Colorisensor, based on the specific inhibition effect of TCh on Fe-PD nanozyme activity, can achieve AChE detection. This proves the AChE analytical feasibility of the colorimetric assay.

To obtain better analytical performance of this Colorisensor, the experimental conditions, including incubation time, incubation temperature, and content ratio of ATCh and AChE, were optimized. As shown in Figure 2C, the relationship between incubation time and the absorbance peak intensity of oxTMB at 652 nm decreased with increasing incubation time,

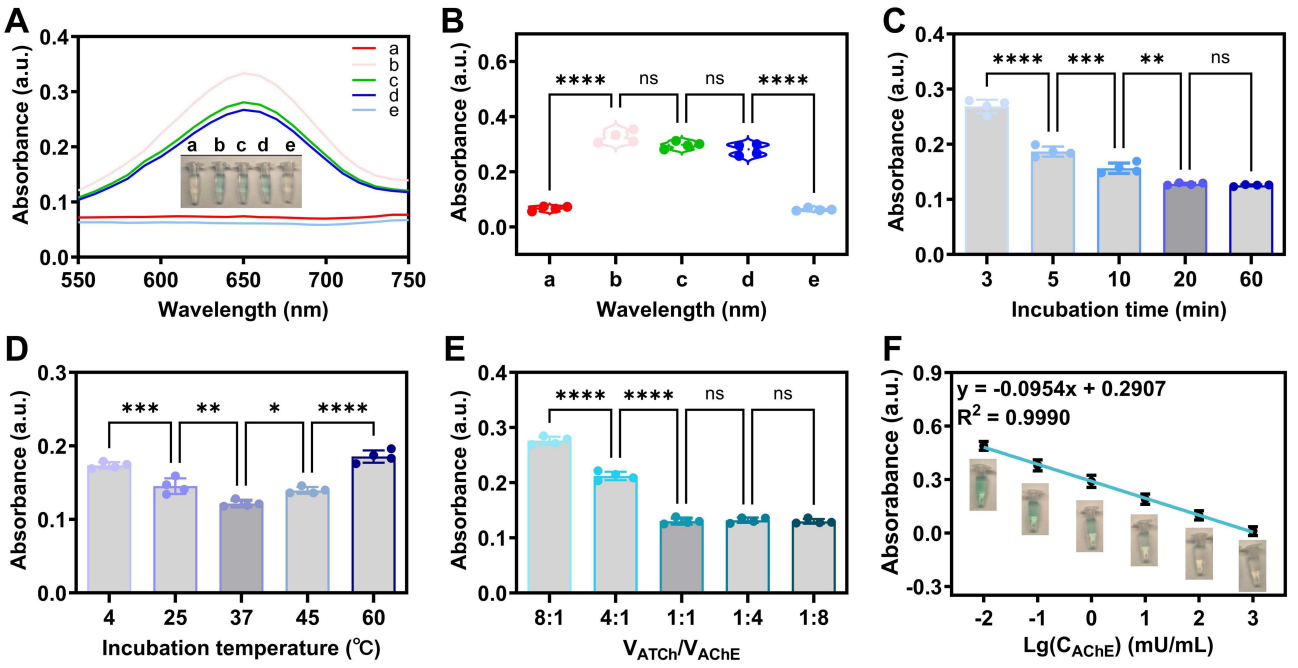

Figure 2 (**A**) UV-vis spectra of the colorimetric biosensing system in the absence and in the presence of AA. The colorimetric biosensing system includes a: TMB + Fe-PD, b: TMB + Fe-PD + H_2O_2, c: TMB + Fe-PD + H_2O_2 + AChE, d: TMB + Fe-PD + H_2O_2 + ATCh, and e: TMB + Fe-PD + H_2O_2 + AChE + ATCh. Inset: corresponding solution color photographs. (**B**) Comparison of the above corresponding absorbance peak intensity. (**C**) Effects of Different incubation time (3 min, 5 min, 10 min, 20 min, and 60 min), (**D**) Different incubation temperature (4 °C, 25 °C, 37 °C, 45 °C, and 60 °C), and (**E**) added volume ratio of ATCh and AChE on the absorbance peak intensity of the Colorisensor system. V_{ATCh} and V_{AChE} represent the added volumes of ATCh and AChE, respectively. (**F**) The relationship calibration curve between the absorbance of the Colorisensor system and the logarithm of the AChE activities (C_{AChE}: from 0.01 to 1000.0 mU/mL) obtained by the Colorisensor. Inset: corresponding solution color photographs. Lg(C_{AChE}) represents the logarithm values of AChE concentration to the base 10. R^2 represents fitting coefficient of the linear relationship curve. Data were expressed as mean ± SD, n = 4, ^{ns}P> 0.05, *P< 0.05, **P< 0.01, ***P< 0.001, ****P< 0.0001.

ranging from 3 to 60 min. When the reaction time was 20 min, the peak intensity almost reached the plateau. Thus, 20 min was chosen as the optimal reaction time. Similarly, reaction temperature and content ratio of ATCh and AChE were also optimized as 37 °C (Figure 2D) and 1:1 (Figure 2E), respectively. Under the optimal experimental conditions, we conducted a detailed analysis of the detection performance of the Colorisensor. Plotting the longitudinal absorbance values versus the logarithm of the AChE activities within the range of 0.01–1000.0 mU/mL (Figure 2F), exhibits a good linear relationship. According to the linear regression equation of y = −0.0954x + 0.2907 (R^2=0.9990), the detection limit of this Colorisensor was estimated as 0.007 mU/mL. Correspondingly, the solution color changed from blue to colorless with the increase of AChE (Inset in Figure 2F), further validating the excellent detection ability of the Colorisensor for AChE activities.

Repeatability, Stability, and Selectivity of This Colorisensor

Before practical analysis, other key detection parameters (including repeatability, stability, and selectivity) of this Colorisensor were tested. As shown in Figure 3A, the relative standard deviation (RSD) of eight independent sensors for 50 mU/mL of AChE detection is about 1.29%, suggesting that the Colorisensor holds outstanding repeatability. To investigate the selectivity of our developed colorimetric biosensing system, several potential interfering substances, including KCl, Glu, L-Cys, GSH, GOx, Lyz, and Tyr, were selected. In Figure 3B, the detection of AChE could not be interfered by these interfering substances, proving that this Colorisensor has excellent selectivity. Prominently, the colorimetric sensor also has long-term storage stability. The RSD of this Colorisensor for 50 mU/mL of AChE detection over 30 days is only 1.83% (Figure 3C). The above results demonstrate the great potential analytical performance of the Colorisensor for the diagnosis of degenerative diseases.

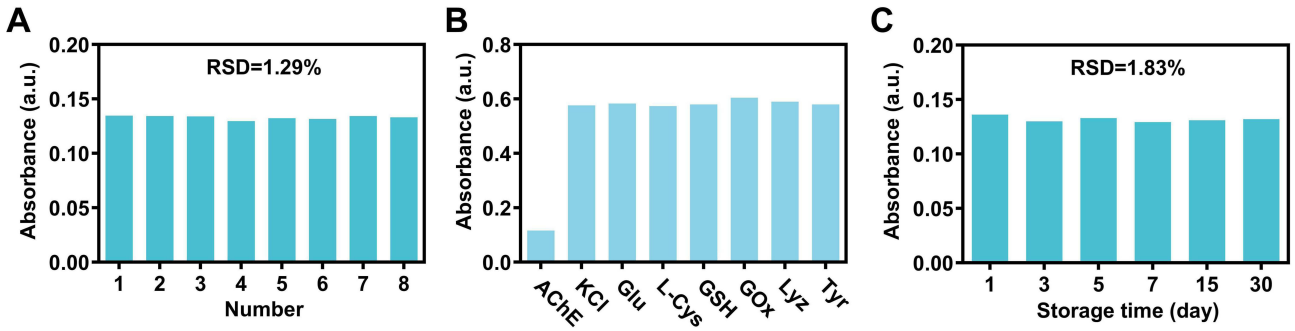

Figure 3 (**A**) Repeatability of eight independent Colorisensors used to detect 50 mU/mL of AChE in AISF. (**B**) Effect of several interferences on the absorbance of the developed Colorisensor at 652 nm in the presence of interferences [KCl (0.15 mM); Glu (4 mM); L-cys and GSH (0.18 mM); GOx, Lyz, and Tyr (50 mU/mL)]; and AChE (50 mU/mL). (**C**) Storage stability of our Colorisensors for 30 days.

Detection of the AChE Inhibitor

Because of the great performance of the colorimetric sensing platform, it was further expanded by exploring its potential application for the determination of AChE inhibitor. Berberine is a promising effective inhibitor of the activity of AChE owing to its neuroprotective effects and treatment of Alzheimer's Disease.[44] As shown in Figure 4A, the absorption intensity gradually increased with increasing berberine concentrations. Figure 4B displayed the trend of inhibition efficiency with berberine concentration ranging from 0.1 to 40.0 μM, which can be determined by the equation: $y = 0.0089x + 0.0418$ (R^2=0.9920). The corresponding solution gradually returned to its blue color of oxTMB. The LOD was 0.034 μM by using the 3σ/slope method, suggesting that the proposed Colorisensor platform was able to achieve berberine detection visually.

POCT Analysis in Simulated Samples by the Microneedle-Based Color-Sensing Array

To evaluate the POCT application in the condition surrounding simulated complex components in vivo, we first constructed the microneedle-based colorisensing array to carry out the actual detection of the activity of target AChE or the inhibiting effects of drug berberine on enzyme activity. The microscopic images of the microneedle array in Figure 5A displayed the well-arranged microneedle structures with uniform morphology, which is the basis for sampling and analyzing biofluid in the sensing platform. To ensure optimal penetration into the skin while minimizing tissue damage, the microneedle arrays were designed with a specific geometry. As shown in Figure 5B, dimensional information of the microneedle array could be provided with their height (H) of 775.4 μm, width (W) of 393.8 μm at the base, and center space (S) of 984.6 μm, ensuring an appropriate size to penetrate the epidermis layer and perform sensing functions. The Colorisensor microneedle array was fabricated via a photopolymerization-micromold method, as Figure 5C exhibited its SEM image for revealing the uniformity and sharpness of the microneedle tips, which are crucial

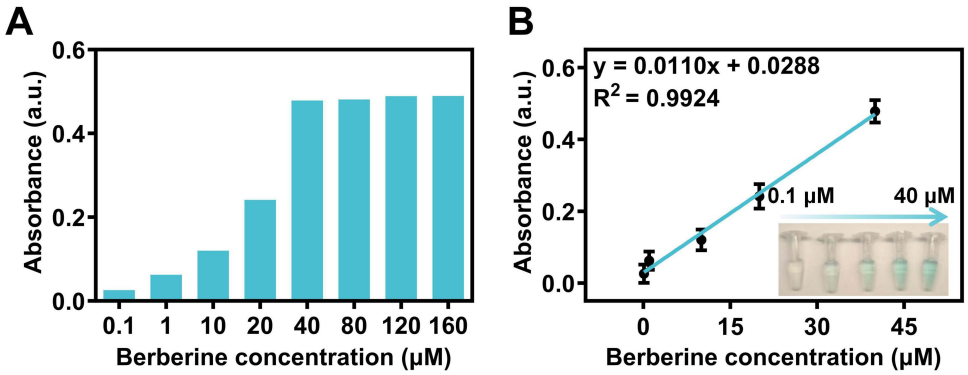

Figure 4 (**A**) Absorbance of the colorimetric system at 652 nm with increasing berberine concentration from 0.1 to 160 μM. (**B**) Corresponding relationship between absorption peak intensity and the berberine concentration (0.1–40 μM). The linear equation: y=0.0089x + 0.0418 (R^2=0.9920).

https://doi.org/10.2147/IJN.S565467

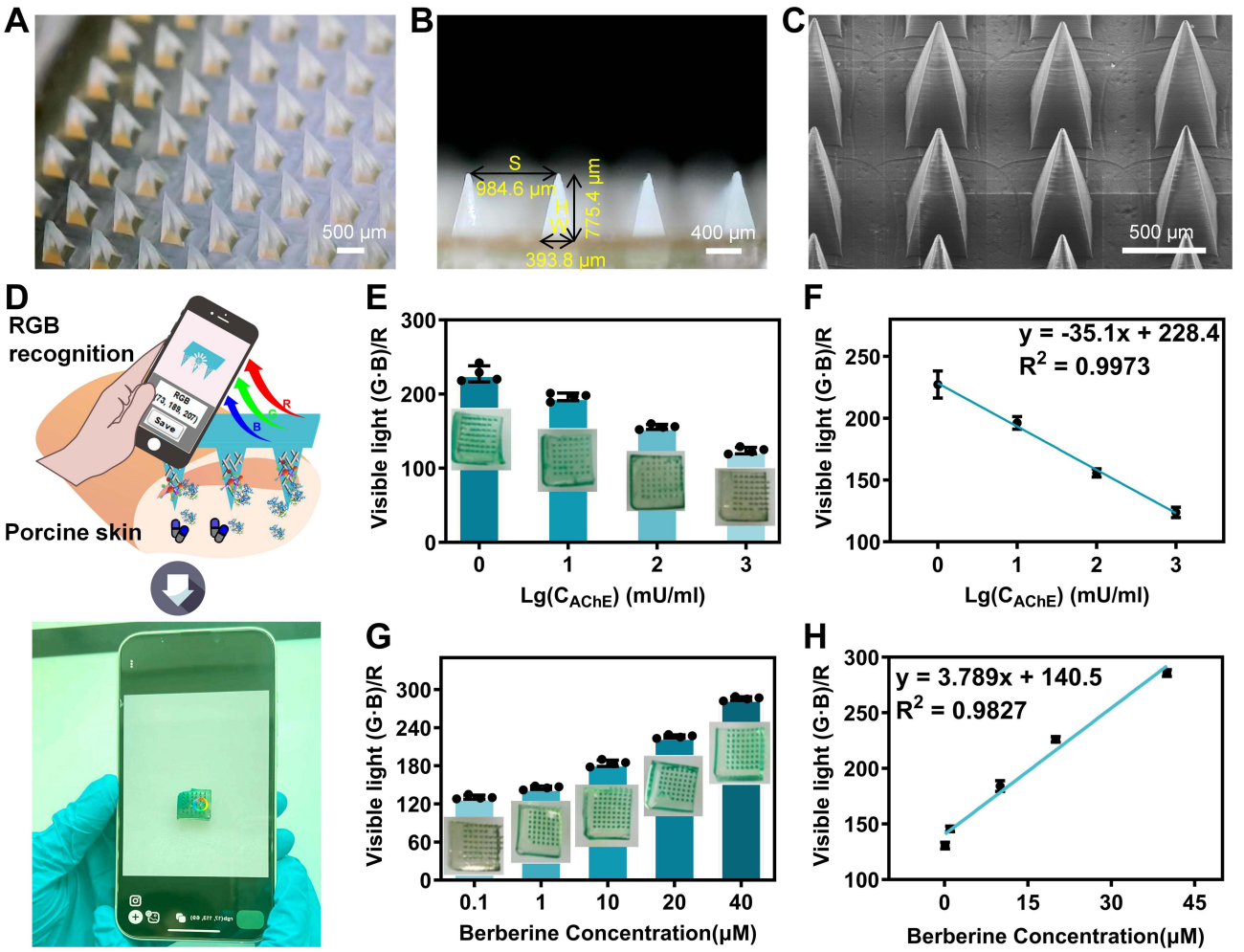

Figure 5 (**A**) microscopic image of part regions, (**B**) Cross-section image of the microneedle sensing array, and (**C**) SEM image of the microneedle sensing array. (**D**) Schematic illustration of Fe-PD nanozyme-mediated colorisensing visual evaluation of AChE activity and its drug inhibitors by the easy-to-use smartphone-assisted microneedle array platform. (**E**) Change of visible light G·B/R values of microneedle arrays with AChE concentrations of 1, 10, 100, and 1000 mU/mL, along with 30 mM of ATCh in porcine ear skin. Inset: Corresponding color photographs of the microneedle arrays. (**F**) Corresponding relationship between Visible light G·B/R values of microneedle arrays and Lg(AChE concentration), with the linear equation of $y = -35.1x + 228.4$ and $R^2 = 0.9873$. (**G**) Change of visible light G·B/R values of microneedle arrays with berberine concentrations (0.1, 1, 10, 20, 40 μM) in porcine skin. Inset: Corresponding color photographs of the microneedle arrays. (**H**) Corresponding relationship between visible light G·B/R values of microneedle arrays and berberine concentration, with the linear equation of $y = 3.789x + 140.5$ and $R^2 = 0.9827$.

for effective contact with tissue fluid. As shown in Figure S3, the microneedle patch was fabricated with a calculated demolding rate of 99.73%. To test the mechanical hardness of the microneedles, we conducted compression mechanical experiments at the speed of 1.0 mm/min to obtaining a force of approximately 0.18 N per needle (Figure S4), which exceeds the transdermal threshold ~0.058 N per needle.[45] The resulting penetration depth of microneedles to pig skin was about 716 μm (Figure S5), indicating their ability to penetrate the stratum corneum and access the dermis layer for analyte detections. To better exhibit the sample ability, we investigated the swelling behavior of the microneedle patch, and defined the water absorption expansion rate as the evaluation index of its swelling performance. As a result, the water absorption expansion rate was calculated as about 156% (Figure S6).

Afterwards, the sampling duration for the microneedle patch was determined through a combination of quantitative in vitro kinetics and ex vivo visual confirmation. We immersed the microneedle patches in artificial interstitial fluid (AISF) and quantitatively monitored the water absorption expansion rate over time. The data indicated that the water absorption expansion rate reached a plateau (the equilibrium stage) after approximately 20 min (Figure S7), suggesting that the patch's fluid uptake capacity was nearly saturated. To corroborate the in vitro findings and visually demonstrate the sampling process, we applied the patches to pig skin. The microneedle patch contains a colorimetric indicator ($CoCl_2$) whose color changes from blue to pink upon

interaction with the extracted interstitial fluid. We observed that the color change progressed gradually and then stabilized, reaching a consistent and unchanging state after a period of 20 minutes (Figure S8). This visual endpoint provided direct evidence that the active sampling process was complete. The strong agreement between the quantitative swelling equilibrium and the qualitative color stabilization gave us high confidence that a 20-min sampling duration is sufficient to ensure the patch operates at its full capacity, guaranteeing complete and efficient sample collection for reliable analysis. The covalent linkage between 3A-PBA and Fe-PD nanozymes minimized the nanozyme detachment, while the low RSD values (2.80%, Figure S9) verified the consistent loading efficiency across batches. The characterization of nanozyme coating stability via continuous washing tests (RSD=3.12%, Figure S10) to further validate the robustness of the modification on the microneedle arrays. To evaluate the actual POCT performance of the Colorisensor platform, we conducted the detection experiment of AChE and its inhibitor on a fresh porcine ear skin as the simulated real in vivo condition, which is reported as a typical in vitro model due to its content of ISF (about 70% of human skin).[46,47] The RGB recognition strategy was employed to quantify the color changes induced by the enzymatic activity of AChE. As depicted in Figure 5D, the microneedle array was applied to the porcine skin spiked with different activities of AChE, and the resulting color changes were captured using a smartphone app. The RGB values were then analyzed to determine the AChE activity. The visible light intensity was defined as (G·B)/R values for quantitative analysis of enzyme activity. As shown in Figure 5E, a clear activity-dependent response to different concentrations of AChE was exhibited. The linear relationship between the logarithm of AChE concentration and the visible light (G·B)/R value is illustrated in Figure 5F, with a correlation coefficient (R^2) of 0.9973. This indicates that the Colorisensor platform can accurately detect AChE activity over a broad range from 0.01 mU/mL to 1000 mU/mL at point-of-care (POC), with a limit of detection (LOD) as low as 0.049 mU/mL. Meanwhile, the developed Colorisensor demonstrates comparable accuracy to the standard Ellman's method under spiked conditions (Figure S11), while exhibiting a wider detection range and a lower detection limit compared to both traditional assays and emerging nanomaterial-based colorimetric methods (Table S4).

To further validate the inhibitor detection utility of the Colorisensor platform, we chose berberine hydrochloride as an inhibitor candidate of AChE. The results presented in Figure 5G and H demonstrate a significant decrease in the visible light intensity (G·B)/R value with increasing concentrations of berberine. The linear regression analysis showed a strong correlation ($R^2 = 0.9827$) between the berberine concentration and the observed color changes from 0.1 μM to 40 μM, with a low LOD of 0.098 μM indicating the high sensitivity and accuracy of the Colorisensor for POC detecting AChE inhibitors.

Potential Applications and Future Perspectives

This study primarily demonstrates the application of our microneedle and nanozyme-based Colorisensor for AChE detection, focusing on its potential in the early diagnosis and drug screening of neurodegenerative diseases. The minimally invasive nature, high sensitivity, and portability of our platform address a critical need for point-of-care monitoring of chronic biochemical changes, such as the subtle fluctuations in AChE activity associated with the onset and progression of conditions like Alzheimer's disease.[48,49]

Beyond this primary focus, we recognize that the significant potential of our platform in other AChE-related testing scenarios. A prominent example is the rapid screening of organophosphate and carbamate pesticide poisoning, where AChE inhibition is a well-established clinical biomarker.[50,51] While current field tests for poisoning are often qualitative, our Colorisensor offers a quantitative, highly sensitive, and user-friendly alternative. It could not only confirm exposure but also help stratify poisoning severity and objectively monitor the efficacy of antidote administration at the point of care, which is crucial in agricultural and low-resource settings. We envision that our Colorisensor will evolve into a multi-scenario POCT tool, capable of addressing diverse needs in both chronic disease management and emergency medicine.

Conclusion

In summary, we develop a highly sensitive acetylcholinesterase assay based on a microneedle-based colorimetric nanosensing platform. Integrating metal-phenol nanozymes with peroxidase-like activity that responds to target-induced changes, and combining smartphone-based RGB color recognition, the platform achieves rapid and easy-to-operate AChE activity detection with a broad linear range of 0.01–1000 mU/mL and excellent selectivity. It successfully identifies berberine as a candidate AChE inhibitor, demonstrating promising potential for applications in drug inhibitor screening fields. Notably, the microneedle-based sensing concept presented herein is a proof-of-concept. To realize point-of-care testing, further engineering

optimizations, such as miniaturization of supporting detection devices, improvement of on-site readout convenience, and enhancement of practical applicability in complex biological scenarios are required. Furthermore, the versatility of this sensing strategy suggests promising potential for expansion into other application fields, such as rapid on-site screening for pesticide exposure, highlighting its broad impact in both clinical and public health settings.

Author Contributions

All authors made a significant contribution to the work reported, whether that is in the conception, study design, execution, acquisition of data, analysis and interpretation, or in all these areas; took part in drafting, revising or critically reviewing the article; gave final approval of the version to be published; have agreed on the journal to which the article has been submitted; and agree to be accountable for all aspects of the work.

Funding

This research was supported by Science and Technology Program of Suzhou (SYW2025037) and Science and Technology Program of Taicang (TC2024JCYL23).

Disclosure

The authors declare no conflict of interest.

References

1. Wang Y, Xue Y, Zhao Q, Wang S, Sun J, Yang X. Colorimetric assay for acetylcholinesterase activity and inhibitor screening based on metal-organic framework nanosheets. *Analy Chem*. 2022;94:16345–16352. doi:10.1021/acs.analchem.2c03290
2. Walczak-Nowicka LJ, Herbet M. Acetylcholinesterase inhibitors in the treatment of neurodegenerative diseases and the role of acetylcholinesterase in their pathogenesis. *Int J Mol Sci*. 2021;22:9290.
3. Liu D-M, Xu B, Dong C. Recent advances in colorimetric strategies for acetylcholinesterase assay and their applications. *TRAC-Trends Anal Chem*. 2021;142:116320. doi:10.1016/j.trac.2021.116320
4. Zhang M, Wang C, Wang Y, Li F, Zhu D. Visual evaluation of acetylcholinesterase inhibition by an easy-to-operate assay based on N-doped carbon nanozyme with high stability and oxidase-like activity. *J Mater Chem B*. 2023;11:4014–4019. doi:10.1039/D3TB00238A
5. Zheng M, Liu M, Ma F, et al. Novel colorimetric-fluorescent dual-mode biosensing platform for detecting acetylcholinesterase and screening acetylcholinesterase inhibitors based on trimetallic nanozymes. *Chem Eng J*. 2025;505:159482. doi:10.1016/j.cej.2025.159482
6. Wan X, Wu P, He X, et al. Nanosilver supported CoAl layered double hydroxide: a high-activity peroxidase-like nanozyme for colorimetric sensing of acetylcholinesterase. *Microchem J*. 2025;215:114321. doi:10.1016/j.microc.2025.114321
7. Zhao Y, Shen A, Hao X, et al. Ultrasensitivity detecting AChE through "covalent assembly" and signal amplification strategic approaches and applied to screen its inhibitor. *Analy Chem*. 2023;95:4503–4512. doi:10.1021/acs.analchem.2c05313
8. Stuetz L, Schulz W, Winzenbacher R. Identification of acetylcholinesterase inhibitors in water by combining two-dimensional thin-layer chromatography and high-resolution mass spectrometry. *J Chromatogr A*. 2020;1624:461239. doi:10.1016/j.chroma.2020.461239
9. Liu Y, Wei X, Chen J, Yu Y-L, Wang J-H, Qiu H. Acetylcholinesterase activity monitoring and natural anti-neurological disease drug screening via rational design of deepeutectic solvents and CeO2-Co(OH)2 nanosheets. *Analy Chem*. 2022;94:5970–5979. doi:10.1021/acs.analchem.2c00428
10. Cheng H, Wang Y, Wang Y, Ge L, Liu X, Li F. A visualized sensor based on layered double hydroxides with peroxidase-like activity for sensitive acetylcholinesterase assay. *Anal Methods*. 2023;15:3700–3708. doi:10.1039/D3AY00776F
11. Qi J-F, Tan D, Wang X-J, et al. A novel acetylcholinesterase biosensor with dual-recognized strategy based on molecularly imprinted polymer. *Sens Actuators B*. 2021;337:129760. doi:10.1016/j.snb.2021.129760
12. Liu X, Zhang X, Wei D, Liu Z, Yang L. Innovative bioinspired hydrogel scaffolds enabling in-situ hybrid nanoflower integration for dual-mode acetylcholinesterase inhibitor profiling. *Biosens Bioelectron*. 2025;271:117032. doi:10.1016/j.bios.2024.117032
13. Grassi J, Frobert Y, Lamourette P, Lagoutte B. Screening of monoclonal-antibodies using antigens labeled with acetylcholinesterase-application to the peripheral proteins of photosystem-1. *Analy Biochem*. 1988;168:436–450. doi:10.1016/0003-2697(88)90341-7
14. Chen Y, Zhang X, Luo X. Enzyme colorimetric cellulose membrane bioactivity strips based on acetylcholinesterase immobilization for inhibitors preliminary screening. *Colloids Surf B*. 2023;223:113184. doi:10.1016/j.colsurfb.2023.113184
15. Yuan Z, Fu M, Wang X, et al. A colorimetric strategy and smartphone-based test strip for the detection of glucose based on the peroxidase activity of a hemin-derived nanozyme. *Anal Methods*. 2025;17:320–329. doi:10.1039/D4AY01878H
16. Anderson S, Shepherd H, Boggavarapu K, Paudyal J. Colorimetric detection of dopamine based on peroxidase-like activity of β-CD functionalized AuNPs. *Molecules*. 2025;30:423. doi:10.3390/molecules30020423
17. Wu J, Wang X, Wang Q, et al. Nanomaterials with enzyme-like characteristics (nanozymes): next-generation artificial enzymes (II). *Chem Soc Rev*. 2019;48:1004–1076. doi:10.1039/c8cs00457a
18. Yan X, Song Y, Wu X, et al. Oxidase-mimicking activity of ultrathin MnO2 nanosheets in colorimetric assay of acetylcholinesterase activity. *Nanoscale*. 2017;9:2317–2323. doi:10.1039/C6NR08473G
19. Li DY, Chen L, Li CY, et al. Nanoplasmonic biosensors for multicolor visual analysis of acetylcholinesterase activity and drug inhibitor screening in point-of-care testing. *Biosens Bioelectron*. 2024;247:115912. doi:10.1016/j.bios.2023.115912

20. Mao Y-W, Zhang J, Zhang R, et al. N-doped carbon nanotubes supported Fe-Mn dual-single-atoms nanozyme with synergistically enhanced peroxidase activity for sensitive colorimetric detection of acetylcholinesterase and its inhibitor. *Analy Chem*. 2023;95:8640–8648. doi:10.1021/acs.analchem.3c01070
21. Guo J, Zhu X, Liang B, et al. Application and recent progress of MXene-based bioactive materials in wound management. *Nano TransMed*. 2025;4:100079. doi:10.1016/j.ntm.2025.100079
22. Ruan H, Zhong Y, Ding H, et al. Dual-continuous microneedle patch integrating transdermal delivery of pH-sensitive licorzinc MOFs and Zn2+ hydrogel sensors for treating alopecia areata. *Chem Eng J*. 2024;499:155961. doi:10.1016/j.cej.2024.155961
23. Ma S, Li J, Pei L, Feng N, Zhang Y. Microneedle-based interstitial fluid extraction for drug analysis: advances, challenges, and prospects. *J Pharm Anal*. 2023;13:111–126. doi:10.1016/j.jpha.2022.12.004
24. Chen Z-B, Luo Y-W, Zhen Y, et al. Advancements in hyaluronic acid cross-linking modalities and implant strategies for mitigating skin aging. *Biomed Eng Commun*. 2025;4:3. doi:10.53388/BMEC2025003
25. Mohammed Y, Kumeria T, Benson HAE, Ali M, Namjoshi S. Skin biomechanics: breaking the dermal barriers with microneedles. *Nano TransMed*. 2022;1:e9130002. doi:10.26599/NTM.2022.9130002
26. Haghayegh F, Norouziazad A, Haghani E, et al. Revolutionary point-of-care wearable diagnostics for early disease detection and biomarker discovery through intelligent technologies. *Adv Sci*. 2024;11:2400595. doi:10.1002/advs.202400595
27. Rabiee N. Revolutionizing biosensing with wearable microneedle patches: innovations and applications. *J Mater Chem B*. 2025;13:5264–5289. doi:10.1039/D5TB00251F
28. Wasilewski T, Kamysz W, Gebicki J. AI-assisted detection of biomarkers by sensors and biosensors for early diagnosis and monitoring. *Biosensors-Basel*. 2024;14:356. doi:10.3390/bios14070356
29. Yuan R, Wang C, Cai J, et al. A rodlike polydopamine-Fe (III) nanozyme-based colorimetric sensor for on-site smartphone readout of ascorbic acid in perishable fruits. *Microchem J*. 2025;208:112318. doi:10.1016/j.microc.2024.112318
30. Lou Z, Zhao S, Wang Q, Wei H. N-doped carbon as peroxidase-like nanozymes for total antioxidant capacity assay. *Analy Chem*. 2019;91:15267–15274. doi:10.1021/acs.analchem.9b04333
31. Cao Y, Chen Y, Zhou Y, Chen X, Peng J. Direct detection of acetylcholinesterase by Fe(HCOO)2.6(OH)0.3. H2O nanosheets with oxidase-like activity on a smartphone platform. *Talanta*. 2024;274:126074. doi:10.1016/j.talanta.2024.126074
32. Zhou Y, Luan T, Fang Q, Zhang Y, Du Y. Molecularly tailored Pd@Pt nanozymes for real-time smartphone-assisted acetylcholinesterase detection and therapeutic inhibitor assessment. *Sens Actuators B*. 2025;440:137889. doi:10.1016/j.snb.2025.137889
33. Zhu Z-R, Huang J-N, Li J-Z, Cao H, Lin Z-Y, Li Y. Janus hydrogel/electrospun-membrane dressing enhancing wound healing in rats. *Biomed Eng Commun*. 2024;3:10. doi:10.53388/BMEC2024010
34. Wang Z, Zou Y, Li Y, Cheng Y. Metal-containing polydopamine nanomaterials: catalysis, energy, and theranostics. *Small*. 2020;16:1907042. doi:10.1002/smll.201907042
35. Liu Q, Wang N, Caro J, Huang A. Bio-inspired polydopamine: a versatile and powerful platform for covalent synthesis of molecular sieve membranes. *J Am Chem Soc*. 2013;135:17679–17682. doi:10.1021/ja4080562
36. Hebbar RS, Isloor AM, Ananda K, Ismail AF. Fabrication of polydopamine functionalized halloysite nanotube/polyetherimide membranes for heavy metal removal. *J Mater Chem A*. 2016;4:764–774. doi:10.1039/C5TA09281G
37. Liu Q, Wang H, Wu C, Wei Z, Wang H. In-situ generation of iron-dopamine nanoparticles with hybridization and cross-linking dual-functions in poly (vinyl alcohol) membranes for ethanol dehydration via pervaporation. *Sep Purif Technol*. 2017;188:282–292. doi:10.1016/j.seppur.2017.06.038
38. Ai Y, Sun H, Gao Z, et al. Dual enzyme mimics based on metal-ligand cross-linking strategy for accelerating ascorbate oxidation and enhancing tumor therapy. *Adv Funct Mater*. 2021;31:2103581. doi:10.1002/adfm.202103581
39. Wang Y, Feng Q, Liu M, et al. S Codoped carbon nanozymes with enhanced peroxidase-like activity and binding affinity for total antioxidant capacity assay. *ACS Appl Nano Mater*. 2023;6:23303–23312. doi:10.1021/acsanm.3c04650
40. Wu Y, Tan X, Gong H, et al. Self-assembled TMB-CuO2 nanosheets for dual-mode colorimetric and NIR-II photothermal detection of uranyl ion. *Anal Chim Acta*. 2025;1356:344041. doi:10.1016/j.aca.2025.344041
41. Gao L, Zhuang J, Nie L, et al. Intrinsic peroxidase-like activity of ferromagnetic nanoparticles. *Nat Nanotechnol*. 2007;2:577–583. doi:10.1038/nnano.2007.260
42. Huang K, Hu C, Tan Q, et al. Nanozymes as a tool to boost agricultural production: from preparation to application. *Environ Sci Nano*. 2025;12:98–120. doi:10.1039/D4EN00780H
43. Ma Y, Chen P, Liao J, Dong XA, He W, Zhang W. Fe3+-induced surface hole generation for selective 'OH formation and efficient NO2 suppression in photocatalytic NO oxidation. *Chem Eng J*. 2025;515:163634. doi:10.1016/j.cej.2025.163634
44. Dan L, Hao Y, Li J, et al. Neuroprotective effects and possible mechanisms of berberine in animal models of Alzheimer's disease: a systematic review and meta-analysis. *Front Pharmacol*. 2024;14:1287750. doi:10.3389/fphar.2023.1287750
45. Chang H, Chew SWT, Zheng M, et al. Cryomicroneedles for transdermal cell delivery. *Nat Biomed Eng*. 2021;5:1008–1018. doi:10.1038/s41551-021-00720-1
46. Samant PP, Prausnitz MR. Mechanisms of sampling interstitial fluid from skin using a microneedle patch. *Proc Natl Acad Sci U S A*. 2018;115:4583–4588. doi:10.1073/pnas.1716772115
47. Yuan R, Cai J, Li J, et al. Integrated microneedle aptasensing platform toward point-of-care monitoring of bacterial infections and treatment. *ACS Sens*. 2025;10:5684–5693. doi:10.1021/acssensors.5c00804
48. Loganathan C, Sakayanathan P, Thayumanavan P. Isolation of bioactive components from Corallocarpus epigaeus tuber and inhibitory potential against various molecular forms of acetylcholinesterase. *Alzheimers Dement*. 2020;16:e043402. doi:10.1002/alz.043402
49. Stavrakov G, Philipova I, Lukarski A, et al. Galantamine-curcumin hybrids as dual-site binding acetylcholinesterase inhibitors. *Molecules*. 2020;25:3341. doi:10.3390/molecules25153341
50. Wille T, Djordjevic S, Worek F, Thiermann H, Vucinic S. Early diagnosis of nerve agent exposure with a mobile test kit and implications for medical countermeasures: a trigger to react. *BMJ Mil Health*. 2020;166:99–102. doi:10.1136/jramc-2019-001310
51. Eyer P, Worek F, Thiermann H, Eddleston M. Paradox findings may challenge orthodox reasoning in acute organophosphate poisoning. *Chem Biol Interact*. 2010;187:270–278. doi:10.1016/j.cbi.2009.10.014